

Characterizing acid diffusion lengths in chemically amplified resists from measurements of deprotection kinetics

Abhijit A. Patil
Yogendra Narayan Pandey
Manolis Doxastakis
Gila E. Stein

Characterizing acid diffusion lengths in chemically amplified resists from measurements of deprotection kinetics

Abhijit A. Patil,^a Yogendra Narayan Pandey,^a Manolis Doxastakis,^{b,*} and Gila E. Stein^{a,*}

^aUniversity of Houston, Department of Chemical and Biomolecular Engineering, 4800 Calhoun Road, Houston, Texas 77204, United States

^bInstitute for Molecular Engineering, Argonne National Laboratory, 9700 South Cass Avenue, Argonne, Illinois 60439, United States

Abstract. The acid-catalyzed deprotection of glassy poly(4-hydroxystyrene-co-*tert*butyl acrylate) films was studied with infrared absorbance spectroscopy and stochastic simulations. Experimental data were interpreted with a simple description of subdiffusive acid transport coupled to second-order acid loss. This model predicts key attributes of observed deprotection rates, such as fast reaction at short times, slow reaction at long times, and a nonlinear dependence on acid loading. Fickian diffusion is approached by increasing the postexposure bake temperature or adding plasticizing agents to the polymer resin. These findings demonstrate that acid mobility and overall deprotection kinetics are coupled to glassy matrix dynamics. To complement the analysis of bulk kinetics, acid diffusion lengths were calculated from the anomalous transport model and compared with nanopattern line widths. The consistent scaling between experiments and simulations suggests that the anomalous diffusion model could be further developed into a predictive lithography tool. © 2014 Society of Photo-Optical Instrumentation Engineers (SPIE) [DOI: 10.1117/1.JMM.13.4.043017]

Keywords: photoresist; stochastic simulations; chemical amplification; lithography; anomalous kinetics; acid trapping; reaction-diffusion; poly(4-hydroxystyrene-co-*tert*butyl acrylate); nonisothermal kinetics; subdiffusive transport.

Paper 14131P received Sep. 4, 2014; accepted for publication Nov. 13, 2014; published online Dec. 16, 2014.

1 Introduction

Chemically amplified resists are essential for high-throughput projection lithography. The intrinsic resolution of these materials is limited by the diffusion length of the acid catalyst in the polymer resin. As feature sizes approach 10 nm, there is significant demand for models that predict spatial extent-of-reaction with nanoscale resolution. It is difficult to construct and validate lithography models because there are few experimental techniques that can visualize acid transport in a reacting photoresist.¹ Instead, several indirect methods have been developed to predict acid diffusion rates at industrially relevant temperatures (i.e., below the photoresist's glass transition). These techniques detect a "signal" that is controlled by diffusion, such as deprotection kinetics^{2,3} or the bulk ionic conductivity.⁴ However, when extracting acid diffusivities from indirect measurements, the outcome will depend on the type of transport model that is selected for data analysis.

A common indirect approach to evaluate acid diffusion is based on a bilayer experiment, where an acid "feeder layer" is placed in contact with a photoresist film. When the bilayer is heated, the acid can diffuse from the feeder layer into the photoresist and catalyze the deprotection reaction. The average extent-of-deprotection is measured with infrared absorbance spectroscopy as a function of time, and these data are employed to determine appropriate parameters for models or simulations that describe the coupled reaction-diffusion process at the macroscopic^{3,5} or mesoscopic² level. For glassy ESCAP (environmentally stable chemical

amplification photoresist)⁶ and APEX⁶ photoresists, the best-fit model parameters predict acid diffusivities on the order of 10^{-14} and 10^{-16} cm²/s in protected^{2,3,5,7} and deprotected^{2,8} resins, respectively, assuming an underlying Fickian transport process. A related approach employs a trilayer sample, where a film of inert deprotected photoresist is sandwiched between an acid feeder layer and a reactive detector layer. When the system is heated, the acid diffuses through the deprotected photoresist to the detector and catalyzes a reaction that is monitored with time-resolved infrared absorbance spectroscopy. Therefore, the acid arrival time in the detector layer is controlled by acid diffusivity and the photoresist layer thickness. The trilayer platform has not been applied at industrially relevant temperatures because acid diffusivities in deprotected photoresist are very low, and with the typical experimental time scales and film thicknesses, the acid arrival time might be too long to be detected.⁹ It is also possible that the acid catalyst is trapped by secondary interactions with the polar-deprotected polymer.³ However, when the deprotected photoresist is heated above its glass transition temperature, then acid arrival is detected and the estimated diffusivities are on the order of 10^{-12} cm²/s.¹⁰ Much like the bilayers, the data are analyzed with the assumption of Fickian transport.

The measured acid diffusion rates in ESCAP and APEX photoresists are extremely low, so it is likely that acid transport will control the deprotection kinetics. However, measured deprotection rates cannot be described with a fast first-order deprotection reaction coupled to slow Fickian transport of the acid catalyst, because the observed deprotection rates are too fast at short times,^{8,10–12} too slow at long

*Address all correspondence to: Gila E. Stein, E-mail: gestein@uh.edu; Manolis Doxastakis, E-mail: edoxastakis@anl.gov

times,^{8,10,12,13} and exhibit a nonlinear dependence on acid concentration.^{12,14} It is possible that reaction kinetics are strongly influenced by the dynamics of a glassy polymer matrix. For example, several studies suggest that acid diffusivities and deprotection rates are reduced in ultrathin photoresist films,^{15–17} which is consistent with suppressed polymer dynamics due to confinement.¹⁸ Therefore, although Fickian transport models are commonly applied, their use might not be justified for these complex materials.

In a recent study, we suggested that acid transport in glassy photoresists can present with anomalous (non-Fickian) character. We measured bulk deprotection rates in a glassy polymer resin (single layer) using time-resolved infrared absorbance spectroscopy, and we interpreted these data with spatially resolved stochastic simulations, where deprotection kinetics was modeled with subdiffusive acid transport coupled to a phenomenological second-order acid loss.¹² This simple approach captured experimental data at all time scales and acid concentrations, and the outcomes were consistent with the extremely slow diffusion rates predicted from bilayer and trilayer experiments. Anomalous transport is common in many classes of condensed soft matter, including examples of probe diffusion in inert polymer glasses, and such behavior is often attributed to spatial heterogeneities in dynamics.^{19,20} The origin of the second-order acid loss remains unclear, but this mechanism is able to describe a broad range of data, so it is most likely associated with the underlying chemistry of these systems. In fact, a recent study of deprotection kinetics in a 193-nm photoresist (2-methyl 2-adamantyl protecting groups) reported a competing reaction pathway (dimerization of by-products) that is responsible for acid loss.²¹

The aims of the present work are (1) to examine the role of polymer dynamics on the anomalous character, and (2) test the predictive capability of our simple model through patterning experiments. To assess the role of polymer dynamics, we introduced an inert plasticizer to increase free volume in the polymer and alter matrix dynamics.²² We anticipated a reduction in the anomalous diffusion behavior, a hypothesis first confirmed with the data presented herein. To evaluate the predictive capability of this model for lithography, we simulated latent image formation using the bulk transport parameters, and then compared these trends with measured line widths in nanopatterned films. The simulated patterning behavior is consistent with experiments, suggesting that this model has the potential to predict resolution limits in chemically amplified resists.

2 Procedures

2.1 Materials

The chemically amplified resists were prepared from the following components: the polymer resin was poly(4-hydroxystyrene-co-*tert*butyl acrylate) (PHOST-PTBA), 60% HOST, supplied by DuPont Electronic Materials. The photoacid generator (PAG) was triphenyl sulfonium perfluoro-1-butanefluoroborate (PFBS) purchased from Sigma Aldrich. Some resist formulas also contained the inert plasticizer dioctyl phthalate (DOP). The PHOST-PTBA, PFBS, and DOP were dissolved in propylene glycol monomethyl ether acetate at the desired concentrations, which are reported relative to the solvent. Typical concentrations for

PHOST-PTBA and DOP were 10 wt.%. All experiments used PFBS concentrations of 1, 2, and 4 wt.%. Substrates were double-side polished p-type silicon wafers (standard resistivity) and were cleaned with Piranha solution prior to use. The glass transition temperature of PHOST-PTBA was measured with spectroscopic ellipsometry, and is $\sim 140^\circ\text{C}$ irrespective of the PFBS or DOP loading. A similar invariance of glass transition temperature with additive loading has been observed in other studies.²³ The glass transition temperature of the deprotected polymer is $\sim 160^\circ\text{C}$.

2.2 Deprotection Experiments

The resists were cast into films that were $\sim 300\text{-nm}$ thick, and then the films were baked at 130°C for 2 min to remove residual solvent. The acid catalyst was fully activated (throughout the depth of the film) by exposing the films to deep ultraviolet light (254 nm) at a dose of $135\text{ mJ}/\text{cm}^2$. Each film was postexposure baked (PEB) at a fixed temperature (either 70, 80, or 90°C) for a specified duration of time, then the changes in chemistry were measured with Brewster angle Fourier-transform infrared (FTIR) spectroscopy. The absorbance at 1149 cm^{-1} , corresponding with the C—O—C stretch of PTBA, was measured for each sample. The absorbance data are used to calculate the deprotection level as a function of time, where the deprotection level is defined as the fraction of TBA groups that were cleaved through the acid-catalyzed deprotection reaction.¹² Each data set is composed of three PFBS concentrations at constant PEB temperature and fixed DOP loading. To analyze each data set (Sec. 2.3), the deprotection profiles for all PFBS concentrations were collapsed onto a master curve by re-scaling the time axis according to $t \times [\text{PFBS}]^n$,¹² where n ranges from 1.3 to 1.6.

2.3 Analysis of Deprotection Experiments

Following the methods reported elsewhere,¹² simulations of reaction coupled to non-Fickian acid diffusion were implemented on a three-dimensional (3-D) lattice ($1\text{ nm}^3/\text{cell}$). Acid was uniformly distributed throughout the simulation volume at concentration levels that correspond with experimental conditions. Acid translations were modeled with a nonergodic, non-Markovian waiting time distribution with long-tail kinetics that reproduces subdiffusive behavior.^{12,24} A key attribute of this effort is the ability to describe the diffusion process with only two parameters, a timescale τ and an anomalous exponent $\gamma < 1$, whose values are determined through comparison with experimental data. The local deprotection reaction was assumed to be instantaneous, because many studies have shown that acid diffusion is the overall controlling step in these systems.^{2,3,5,7,10} An acid annihilation mechanism is needed to fit the experimental data for long times. This acid loss mechanism follows second-order kinetics and is implemented following a simple rule where two acids in the same cell combine to form one unit (see Fig. 1). The simulations were fit to each experimental data set (master curve) using a simulated annealing algorithm with the adjustable parameters τ and γ . Fifty runs were performed for each data set, and within each run, 200 simulations were performed to evaluate residuals and guide the optimization process. This feature of the analysis underlines the need for numeric models that are rapidly evaluated to assess the relevant parameters. The best-fit values of γ and τ can describe all acid loadings and are only a function of

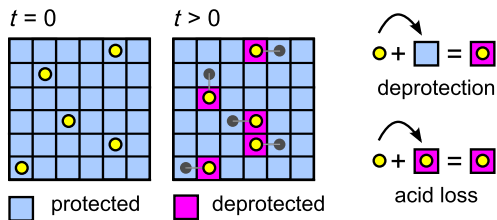


Fig. 1 Simulation algorithm illustrated in two-dimensions for clarity.

PEB temperature and DOP loading (i.e., the same parameters can describe all acid concentrations). The optimization algorithm employed $30 \times 30 \times 30$ cells, while the final simulated deprotection profiles in Fig. 3 were generated with $50 \times 50 \times 50$ cells. Error bars represent ± 1 standard deviation. It is important to emphasize that more complex mathematical schemes with additional parameters are straightforward to implement, but our data suggest that the previously described methods are sufficient to capture the observed behavior at industrially relevant length and time scales. Furthermore, noise in the experimental data hinders reliable application of more complex models with additional parameters.

2.4 Nanopatterning

Resist films (330 to 370-nm thick) containing 4 wt.% PFBS, with and without 10 wt.% DOP, were patterned with single-pass lines using electron beam lithography (EBL). The beam voltage and current were 50 kV and 100 pA, respectively, and a 5-nm shot pitch was employed. The dose was varied from 450 to 800 $\mu\text{C}/\text{cm}^2$ in increments of 50 $\mu\text{C}/\text{cm}^2$. The pattern layout was designed to minimize proximity effects: each patterned region was composed of 20 lines that were 3- μm -long on a 1.5- μm pitch. Adjacent regions were separated by 15 μm of empty space (along x or y axes). The conditions for PEB were 90°C and 30 s. Patterns were developed in 0.1-N tetramethylammonium hydroxide for 30 s, then rinsed in deionized water and dried under nitrogen flow. Patterns were sputter coated with ~ 4 nm of tungsten and imaged with a scanning electron microscope (SEM) under the following conditions: accelerating voltage 15 kV, working distance of 5 mm, and magnifications in the range of 150 to 250 k. Average line widths were calculated from at least three images per dose using an edge-detection routine implemented in MATLAB®. Error bars represent ± 1 standard deviation.

2.5 Simulations of Nanopattern Formation

Simulations of nanopattern formation were implemented on a 3-D lattice of $100 \times 100 \times 100$ cells (1 nm^3/cell). The initial spatial distribution of the PFBS catalyst (illustrated in Fig. 2) was selected from a Gaussian probability function and introduced at the center of the simulation system. The full-width at half-maximum was fixed at 19 nm, which was calculated by assuming a 4-nm diameter electron beam (per instrument manufacturer) broadened by 15 nm of forward scattering (330-nm-thick resist at 50 kV).^{25,26} We did not include proximity effects due to low-angle backscattering because the line patterns in experiments were sparse. The number of acid particles assigned to the lattice was determined by the average PFBS concentration in experiments (4 wt.%, or 0.05/ nm^3). The reaction-diffusion model was implemented as described in Sec. 2.3. The total

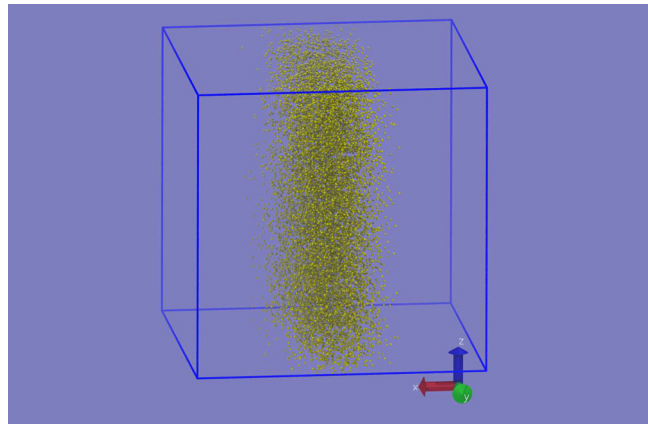


Fig. 2 Initial spatial distribution of PFBS catalyst for nanopatterning simulations.

reaction time was set at 30 s, and the transport parameters τ and γ were fixed based on the best-fit results from analysis of bulk deprotection data at 90°C.

3 Results and Discussion

The experimental and simulated deprotection levels for glassy resists without DOP are compared in Figs. 3(a)–3(c) for PEB conditions of 70°C, 80°C, and 90°C. Each PEB condition includes three PFBS loadings of 1, 2, and 4 wt.%. In all cases, the deprotection rate quickly rises at short-to-intermediate PEB times, but decelerates at long times. Similar behavior is observed in experiments by other research groups, and as discussed in our prior work, these features are not provided by Fickian diffusion coupled to first-order deprotection and/or first-order acid trapping reactions.¹² Fickian diffusion always under-estimates the deprotection level at short times, and first-order acid trapping cannot describe the long-time behavior for all PFBS concentrations. However, the anomalous transport model with acid-acid annihilation offers near-quantitative agreement with experimental data, although some deviations persist at very long PEB times (ca. >2 h). The deviations at long times may result from slow environmental contamination that deactivates the acid catalyst, or perhaps a gradual densification of the film that reduces the rates of acid transport. In any case, the long time limit is not relevant for industrial applications. Most importantly, the model captures kinetics for all PFBS concentrations, so outcomes can then be scaled to higher PFBS loadings that are representative of industrial formulations.

The effect of PEB temperature on best-fit model parameters (τ, γ) is summarized in Figs. 4(a) and 4(b). (These values are slightly different than reported in our previous work that included experimental data up to 10 wt.% PFBS loading.¹² We no longer consider high PAG loadings because the deprotection rates are too fast for reliable measurement with our *ex-situ* FTIR protocol.) First, we note that increasing the PEB temperature produces a corresponding increase in the deprotection rate. This behavior is summarized in Fig. 4(a), which reports the diffusion-controlled reaction rate ($1/\tau$) as a function of inverse temperature ($1/T$). The scaling is consistent with Arrhenius kinetics, although more data points are required to distinguish between Arrhenius kinetics and the Williams–Landel–Ferry model that is common for glassy polymers.^{8,14} Second, we find that γ increases with

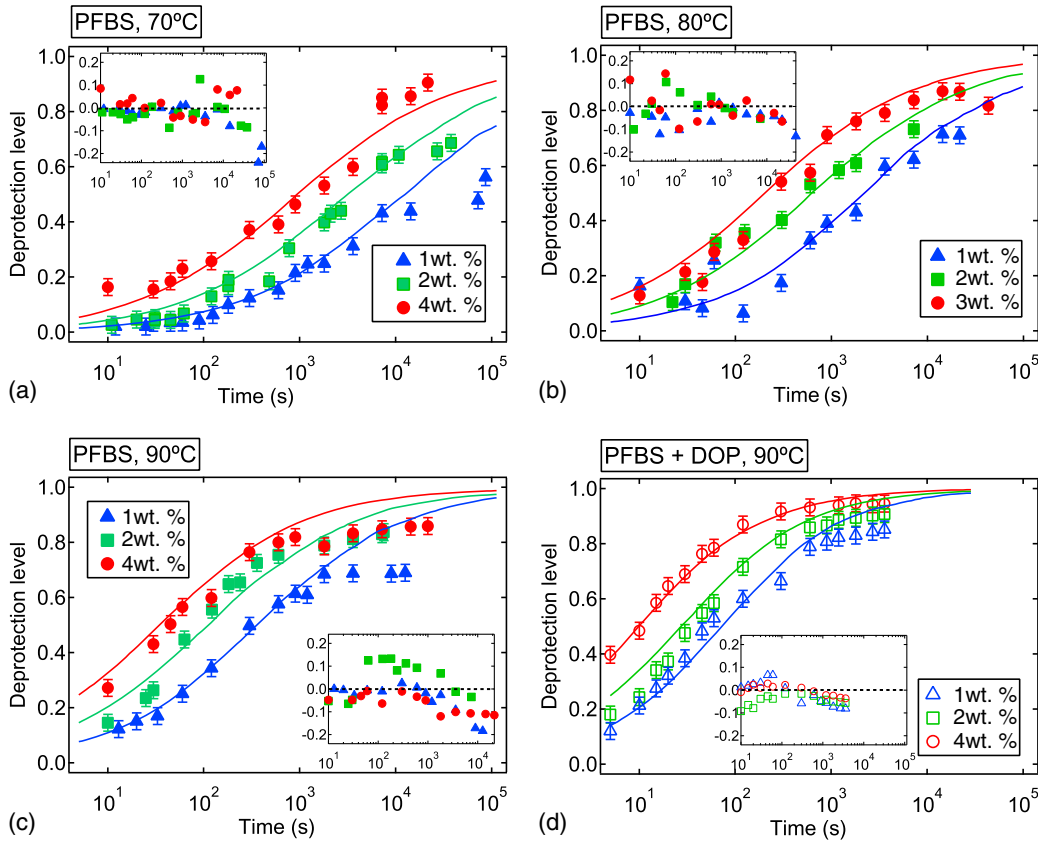


Fig. 3 Experimental deprotection levels (symbols) and best-fit simulations (lines) for 1, 2, and 4 wt.% acid loading. (a) 70°C, (b) 80°C, (c) 90°C, and (d) 90°C with 10 wt.% dioctyl phthalate (DOP).

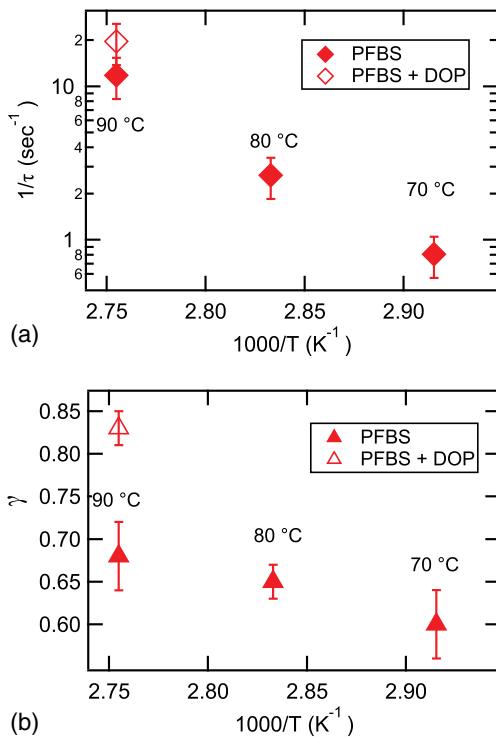


Fig. 4 (a) Deprotection rate $1/\tau$ as a function of temperature; (b) anomalous exponent γ as a function of temperature. Note that $\gamma < 1$ reproduces subdiffusive transport, while $\gamma = 1$ represents Fickian transport.

PEB temperature, meaning the model approaches Fickian character at higher temperatures (note that $\gamma \rightarrow 1$ reproduces Fickian transport). This behavior is reported in Fig. 4(b). The values of γ fall in the range of 0.6 to 0.8, which is consistent with studies of isothermal probe diffusion in inert polymer glasses.^{20,27}

The observed anomalous kinetics could be associated with transient free volume generation,^{10,28} plasticization from volatile reaction by-products,^{10,28} nonisothermal effects,⁸ and coupling between acid transport and local heterogeneities in polymer dynamics.¹² Transient free volume and by-product plasticization were rigorously examined for poly(*tert*butoxycarbonyl-oxystyrene) resins, and these studies determined that neither factor is controlling the reaction kinetics.²⁹ Nonisothermal effects may be relevant, as the exothermic heat of reaction could increase the temperature within the film and enhance the diffusion rate. Further studies are underway to examine this hypothesis. In the present study, we considered the effects of polymer dynamics on reaction kinetics. We incorporated the plasticizer DOP to increase free volume in the polymer film, and the impact on deprotection rates is seen by comparing Figs. 3(c) and 3(d). Although these experiments were performed with the same PEB temperature, the deprotection rates are visibly enhanced by DOP, suggesting that the acid-counterion pair can diffuse more rapidly throughout the plasticized polymer film. The best-fit values of τ and γ for resists with DOP are reported in Figs. 4(a) and 4(b): the deprotection rate is ~66% faster with DOP, and the anomalous exponent γ is increased from

~0.7 to 0.8. The latter point is particularly interesting, because the increase in anomalous exponent points to a shift in the underlying time-dependent diffusion mechanism. One possible explanation for this behavior is a nonisothermal effect, where faster diffusion in the plasticized film leads to increased deprotection rates, and a corresponding increase in the heat effect then further accelerates the diffusion. An alternative explanation is that plasticization by DOP increases the average diffusion rate and also reduces the coupling between transport and local heterogeneities. Although we cannot definitively identify a sole underlying cause of anomalous kinetics, it is clear that dynamical properties in the polymer resin play an important role in the reaction-diffusion mechanism.

A question that remains is whether the parameters extracted from bulk analysis can predict lithographic properties. We exposed line patterns in each resist formula using EBL, and then compared experimental outcomes with simulations of nanopattern formation. For experiments, resists with 4 wt.% PFBS (with and without DOP) were patterned by EBL (sparse, single-pass lines). The postexposure bake was implemented at 90°C for 30 s, and then patterns were developed for 30 s to form a relief image of long trenches (with depths equal to resist thickness). The widths of these line patterns (trenches) were measured with SEM. Simulations were devised to match EBL experiments: The reaction-diffusion model was implemented with the best-fit values of γ and τ for each resist formula at 90°C, which are summarized in Fig. 4. The initial spatial distribution of acid was based on an average 4 wt.% acid loading and incorporated the forward electron scattering through a 330-nm-thick resist film. The simulated reaction time was 30 s.

Representative SEM images of developed line patterns are reported in Fig. 5(a). Measured line widths are summarized in Fig. 5(b) as a function of DOP loading and electron beam dose, where each data set (symbols connected by lines) reflects the outcomes of an individual patterning experiment. There is scatter among data sets, but it is clear that adding DOP will increase the line width (by a factor of 1.5 to 3). This is qualitatively consistent with analysis of bulk experiments, as we observed increased deprotection levels with the addition of DOP (0.7 compared with 0.5 after 30 s at 90°C). A higher deprotection level is expected to enhance the dissolution kinetics. However, we note that resist solubility differs for formulas with and without DOP, and the solubility also controls the dissolution kinetics and ultimate line widths. Resist solubility was evaluated by immersing bulk films with varying deprotection levels in the developer for 30 s. The thickness of the film was measured before (t_i) and after (t_f) development. Figure 5(c) reports the normalized residual thickness (NRT = t_f/t_i) as a function of average deprotection level. These data demonstrate that DOP, a nonpolar additive, inhibits dissolution in the polar developer, but the solubility switch is effected at low deprotection levels in both formulas. These observations underline the need to couple simulations of pattern formation with models for dissolution that reflect the resist composition, which is a direction for future work.

The image maps in Fig. 6(a) show simulated deprotection profiles averaged along the z -axis (through the film thickness). The color scale illustrates the transition from no deprotected sites (blue) to a maximum deprotection level of 0.7

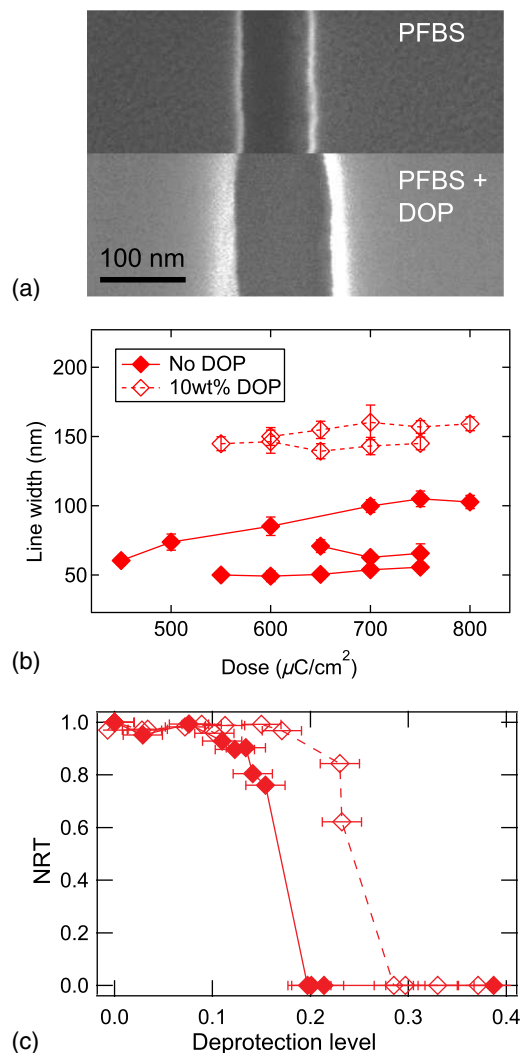


Fig. 5 (a) Examples of scanning electron microscope measurements for each formula, exposure dose of 600 $\mu\text{C}/\text{cm}^2$. (b) Line width for each resist formula as a function of exposure dose. (c) Normalized residual thickness (NRT) for each resist formula as a function of deprotection level (30-s development).

(red), and the solid black contour marks an average deprotection level of 0.33. The line profiles in Fig. 6(b) report the initial acid distribution and final deprotection levels averaged along both z and x axes. The simulations predict image blur due to acid diffusion in both formulas, but this effect is more pronounced for resists that include DOP. The simulations also predict that DOP will generate a higher level of deprotection near the center of the line.

The measured line widths are larger than those predicted by simulations, but there are several reasons why quantitative agreement is not anticipated at this stage. First, the simulations do not account for proximity effects due to electron backscatter in EBL. Considering the sparse pattern layout in experiments, we do not anticipate a large proximity effect. However, the data in Fig. 5(c) demonstrate that very low deprotection levels can effect the solubility switch, so even a small amount of activation due to low-angle backscattering could impact the tails of the latent images. Second, the resist/developer system offers very poor lithographic contrast and is, therefore, not a great model for patterning

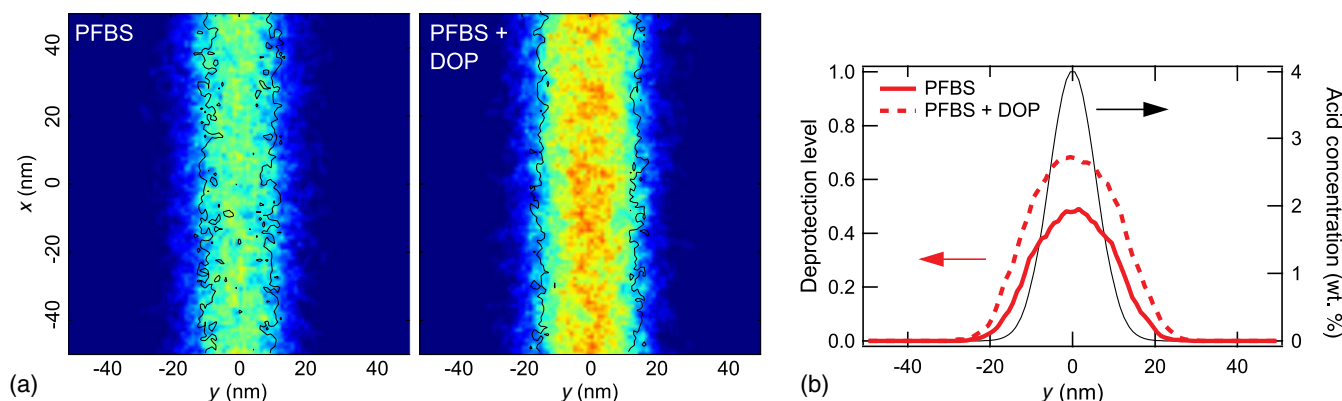


Fig. 6 (a) Image maps of simulated deprotection level (averaged through film thickness) for 30-s post-exposure bake at 90°C. (b) Deprotected line width at 30 s and initial spatial density of acid catalyst.

experiments (as evidenced by the large variance in measured line widths). Third, and most importantly, the simulations do not include a model for resist dissolution. Experiments demonstrate that DOP reduces the solubility of the polymer in the developer [Fig. 5(c)], so one might expect slower dissolution at the “tails” of the latent image (where deprotection levels are low). However, the model predicts that DOP will increase the deprotection level (Fig. 6), and this factor might enhance dissolution rates near the center of the line.

4 Conclusions

The acid-catalyzed deprotection of glassy photoresists was measured with FTIR spectroscopy as a function of PEB time, acid loading, and PEB temperature. Data were interpreted with a simple and accurate model based on subdiffusive acid transport coupled to a second-order acid loss. The model can describe experimental data that span a wide range of time scales and acid concentrations, with only two temperature-dependent fitting parameters: a characteristic time scale for acid translations (τ), and an anomalous exponent (γ) that reflects the deviations from Fickian transport (specifically, the underlying non-Gaussian distribution of acid hopping times). We demonstrated that anomalous kinetics are influenced by the dynamical properties of the polymer resin, which was verified by adding plasticizing agents to the resist, and we discussed other factors that might be relevant (such as nonisothermal effects). Finally, we presented patterning data where the measured line widths were in qualitative agreement with simulated latent images. We conclude that lithographic resolution might be predicted from simple FTIR measurements coupled to spatially resolved simulations. Future experiments will evaluate bulk deprotection rates and nanopattern formation in resists with higher contrast, and simulations will be adapted to incorporate models for resist dissolution.

Acknowledgments

The authors acknowledge past funding from the Semiconductor Research Corporation that helped to initiate this research program (Contract No. 2011-OJ-2128), as well as current funding from the National Science Foundation (Grant No. CBET-1437878 to G.E.S., and Grant No. CBET-1067356 to M.D.). The authors thank Professor Vemuri Balakotaiah for helpful discussions regarding nonisothermal effects in diffusion-controlled reactions. The

authors also thank DuPont Electronic Materials for supplying the P(HOST-co-TBA) resin.

References

1. A. J. Berro et al., “Super-resolution optical measurement of nanoscale photoacid distribution in lithographic materials,” *ACS Nano* **6**, 9496–9502 (2012).
2. G. M. Wallraff et al., “Experimental method for quantifying acid diffusion in chemically amplified resists,” *Proc. SPIE* **3678**, 138–148 (1999).
3. S. Kang et al., “Characterization of the photoacid diffusion length and reaction kinetics in EUV photoresists with IR spectroscopy,” *Macromolecules* **43**(9), 4275–4286 (2010).
4. C. M. Berger and C. L. Henderson, “Improved chemically amplified photoresist characterization using interdigitated electrode sensors: photoacid diffusivity measurements,” *Proc. SPIE* **5376**, 392–403 (2004).
5. S. Kang et al., “A comparison of the reaction-diffusion kinetics between model-EUV polymer and molecular-glass photoresists—art. no. 692317,” *Proc. SPIE* **6923**, 692317 (2008).
6. H. Ito, “Chemical amplification resists for microlithography,” in *Microlithography-Molecular Imprinting*, Vol. 172 of *Advances in Polymer Science*, pp. 37–245, Springer Berlin, Heidelberg (2005).
7. M. D. Stewart et al., “Acid catalyst mobility in resist resins,” *J. Vac. Sci. Technol. B* **20**, 2946–2952 (2002).
8. M. D. Stewart et al., “Study of acid transport using IR spectroscopy and SEM,” *Proc. SPIE* **3999**, 665–674 (2000).
9. M. D. Stewart, “Catalyst diffusion in positive-tone chemically amplified photoresists,” PhD Thesis, Copyright UMI—Dissertations Publishing (2003).
10. S. V. Postnikov et al., “Study of resolution limits due to intrinsic bias in chemically amplified photoresists,” *J. Vac. Sci. Technol. B* **17**, 3335–3338 (1999).
11. T. Kozawa et al., “Impact of nonconstant diffusion coefficient on latent image quality in 22 nm fabrication using extreme ultraviolet lithography,” *J. Photopolym. Sci. Technol.* **21**(3), 421–427 (2008).
12. G. M. Perera et al., “Reaction kinetics in acid-catalyzed deprotection of polymer films,” *J. Phys. Chem. C* **116**, 24706–24716 (2012).
13. B. D. Vogt et al., “Measurements of the reaction-diffusion front of model chemically amplified photoresists with varying photoacid size,” *Macromolecules* **39**(24), 8311–8317 (2006).
14. B. Jung et al., “Kinetic rates of thermal transformations and diffusion in polymer systems measured during sub-millisecond laser-induced heating,” *ACS Nano* **6**, 5830–5836 (2012).
15. D. S. Fryer, P. F. Nealey, and J. J. de Pablo, “Scaling of T-g and reaction rate with film thickness in photoresist: a thermal probe study,” *J. Vac. Sci. Technol. B* **18**, 3376–3380 (2000).
16. D. L. Goldfarb et al., “Confinement effects on the spatial extent of the reaction front in ultrathin chemically amplified photoresists,” *J. Vac. Sci. Technol. B* **19**, 2699–2704 (2001).
17. L. Singh, P. J. Ludovice, and C. L. Henderson, “Effect of nanoscale confinement on the diffusion behavior of photoresist polymer thin films,” *Proc. SPIE* **5376**, 369–378 (2004).
18. D. B. Hall and J. M. Torkelson, “Small molecule probe diffusion in thin and ultrathin supported polymer films,” *Macromolecules* **31**, 8817–8825 (1998).
19. M. T. Cicerone, F. R. Blackburn, and M. D. Ediger, “Anomalous diffusion of probe molecules in polystyrene: evidence for spatially heterogeneous segmental dynamics,” *Macromolecules* **28**(24), 8224–8232 (1995).

20. C.-Y. Wang and M. D. Ediger, "Anomalous translational diffusion: a new constraint for models of molecular motion near the glass transition temperature," *J. Phys. Chem. B* **104**(8), 1724–1728 (2000).
21. B. Jung et al., "Laser-induced sub-millisecond heating reveals distinct tertiary ester cleavage reaction pathways in a photolithographic resist polymer," *ACS Nano* **8**(6), 5746–5756 (2014).
22. A. A. Patil, M. Doxastakis, and G. Stein, "Modeling acid transport in chemically amplified resist films," *Proc. SPIE* **9051**, 90511M (2014).
23. D. S. Fryer et al., "Study of acid diffusion in resist near the glass transition temperature," *J. Vac. Sci. Technol. B* **17**, 3351–3355 (1999).
24. I. M. Sokolov, "Models of anomalous diffusion in crowded environments," *Soft Matter* **8**, 9043–9052 (2012).
25. T. H. P. Chang, "Proximity effect in electron-beam lithography," *J. Vac. Sci. Technol.* **12**(6), 1271–1275 (1975).
26. G. Owen, "Methods for proximity effect correction in electron lithography," *J. Vac. Sci. Technol. B* **8**, 1889–1892 (1990).
27. J. T. Bendler and M. F. Shlesinger, "Derivation of the Kohlrausch-Williams Watts decay law from activation-energy dispersion," *Macromolecules* **18**(3), 591–592 (1985).
28. E. Croffie, M. S. Cheng, and A. Neureuther, "Moving boundary transport model for acid diffusion in chemically amplified resists," *J. Vac. Sci. Technol. B* **17**, 3339–3344 (1999).
29. W. D. Hinsberg et al., "Product volatilization as a probe of the physics and chemistry of latent image formation in chemically amplified resists," *J. Phys. Chem. A* **106**, 9776–9787 (2002).

Abhijit A. Patil is currently a PhD candidate in chemical engineering at the University of Houston. He received his bachelor's degree from the University of Mumbai, India (2007), and a master's degree from the University of Kentucky (2009), both in chemical engineering. His research at the University of Houston is focused on measuring reactions in chemically amplified photoresists to develop predictive models for pattern formation. He is interested applying concepts from polymer physics to electronic materials and nanolithography.

Yogendra Narayan Pandey received his bachelor of technology in chemical engineering from the Institute of Technology, Banaras Hindu University, Varanasi, India, in 2005. He received his PhD degree in chemical engineering in 2013 from the University of Houston, Houston, Texas. He worked with Professor Manolis Doxastakis on developing simulation methods for modeling of materials, e.g., polymer–nanocomposites, polymer thin films, and zeolites. He currently works with Halliburton as a senior technical professional in Houston, Texas.

Manolis Doxastakis is a materials scientist at the Institute of Molecular Engineering at Argonne National Laboratory. His research is focused on developing simulation methods to study equilibrium structures, fluctuations, and dynamics of multicomponent systems at interfaces. He received his diploma in chemical engineering from the National Technical University of Athens in 1996 and an MSc in materials science and PhD degree in chemical engineering from University of Patras in 2002.

Gila E. Stein is the Ernest J. and Barbara M. Henley assistant professor of chemical and biomolecular engineering at the University of Houston. Her research is focused on the physics and chemistry of thin polymer films, emphasizing challenges that are relevant for polymer-based electronic materials such as block copolymers, polymer blends, photoresists, and polymer semiconductors. She received BS and PhD degrees in chemical engineering from Drexel University and the University of California (Santa Barbara) in 2002 and 2006, respectively, and was a National Research Council post-doctoral fellow at the National Institute of Standards and Technology from 2007 to 2008.